

Hybrid CFD/ low order modelling of thermoacoustic limit cycles

By **S. Jaensch, M. Merk, E. A. Gopalakrishnan[†], S. Bomberg, T. Emmert, R. I. Sujith[†] AND W. Polifke**

Professur für Thermofluidynamik, Technische Universität München, Garching, Germany

[†] Department of Aerospace Engineering , Indian Institute of Technology Madras , Chennai , India

This paper proposes and compares two nonlinear time-domain models of self-excited thermoacoustic instabilities of laminar premixed flames. We resolve the flame and its immediate vicinity with a CFD simulation. Simultaneously, the acoustic field is modeled with a low-order model that is coupled to the CFD over the inlet boundary condition. The first model is based on a fully compressible CFD solver. Here, the low-order model describes the plenum of the combustor and is coupled via the characteristic wave amplitudes using the newly developed Characteristic Based State-Space Boundary Conditions. This reduces the computational costs and allows to change the plenum length of the combustor without changing the computational grid. The second model resolves the flame with an incompressible CFD solver. In order to include the thermoacoustic feedback this model is coupled on-line with an acoustic network model over the global heat release rate and an acoustic reference velocity according to the Rankine-Hugoniot equations. A bifurcation analysis using the plenum length as bifurcation parameter is conducted. Both models exhibit complex nonlinear oscillations. A comparison in terms of a root mean square (RMS), dominant frequency, power spectrum and phase portraits show that both models are in good agreement.

1. Introduction

The development of gas turbines or rocket engines is often limited by thermoacoustic instabilities. A strong interaction between the unsteady heat release of the combustion with the acoustic field yields very large oscillations in pressure, heat release and velocity. These oscillations can reach amplitude levels at which gas turbine have to be shut down or rockets are destroyed. In order to decide whether an thermoacoustic instability reaches such amplitude levels nonlinear models are required, which are capable of predicting thermoacoustic limit cycles.

In order to get a better understanding of the interaction between combustion and acoustic, the investigation of thermoacoustic instabilities of laminar flames is still a topic of ongoing research. Kabiraj et al. [1] studied a laminar matrix burner which was positioned in a tube. Changing the position of the flame inside the duct, periodic, aperiodic, or chaotic oscillations as well as hysteresis was observed. The flame describing function (FDF) [2, 3] together with an acoustic network model has been shown to provide a useful estimate of limit cycle amplitudes in many cases. However, it is a frequency domain approach and considers only a single unstable acoustic mode. Therefore, it can only predict harmonic instabilities. The advantage of time-domain models is

that they can account for multi-model coupling, which is necessary to describe all complex types of oscillations observed. A time-domain model that has drawn recent interest uses a G-equation based flame model coupled with a low-order acoustic model [2, 4–6]. This model shows complex nonlinear oscillations, however, no quantitative agreement with experimental results is achieved. Several possible reason for this mismatch can be found: The G-equation flame model, the linear low-order acoustic model, the coupling between these models or other effects, such as conjugated heat-transfer or uncertainties in the flow properties.

In the present study we compare self-excited thermoacoustic instability of a fully compressible and an incompressible CFD simulation. The compressible simulation resolves the flame acoustic interaction and also a possible nonlinear scattering of acoustic waves at the perforated plate stabilizing the flame. Therefore, this simulation serves as reference. So far such simulations have been considered as too expensive to conduct a bifurcation analysis. In the present study we minimize the computational costs using the newly developed characteristic based state-space boundary conditions (CBSBC) [7]. The incompressible simulation, on the other hand, suppresses all acoustic effects inside the computational domain. It is coupled with a low order acoustic model in order to exhibit thermoacoustic instabilities. This coupling is similar to the coupling of an acoustic model with the G-equation used in [6]. A bifurcation analysis using the plenum length as bifurcation parameter shows that both simulations are in good quantitative agreement. A more detailed look at the oscillations observed at two specific plenum length, shows that both simulations exhibit the same type of oscillations. This allows us to exclude an insufficient acoustic model and an incorrect coupling from the list of possible reasons for the mismatch of the G-equation based model with the experimental data.

The models investigated in the present study form a basis for further research. On the one hand they can be compared with experimental results and if necessary be extended. On the other hand they can serve as reference for nonlinear low-order models for the flame dynamics.

The rest of the paper is structured as follows: In the next section we explain the models investigated. In section 3, the numerical results are presented. In section 4 we summarize the outcome of the summer program and give an outlook on further work.

2. Numerical setup

The laminar slit burner considered in the present study is shown in Fig. 1. Kornilov et al. [8] and Duchaine et al. [9] investigated the linear dynamic of this configuration. Good agreement between experimental and numerical results was described. The CFD domain represents only one half of a flame. Consequently, symmetry boundary conditions are used at the left and right boundaries. At the inflow we impose a mean velocity of 0.4 m/s and a temperature of 293 K . The solid wall are modeled as Dirichlet boundary condition with a temperature of 373 K . The fuel is Methane with an equivalence ratio of 0.8. For a detailed description of the reaction mechanism we refer to [9]. As sketched in Fig. 1, a structured grid with 122300 cells was utilized. In the region of the steady-state position of the flame and of the area contractions the grid is uniform with a cell size of 0.025 mm . Outside the region grading in axial direction was applied in order to reduce the number of cells.

In order to model thermoacoustic instabilities of the configuration correctly, it is crucial to capture the coupling between the fluctuating heat release rate and the acoustic field.

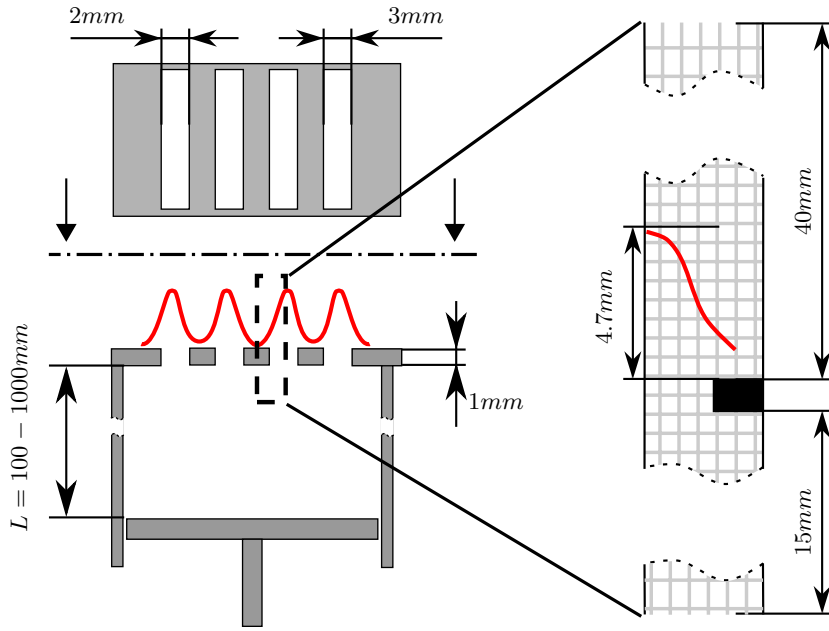


FIGURE 1. Left: Sketch of the experimental configuration considered. Right: Truncated CFD domain.

Here, the treatment of the compressible and the incompressible simulation differs and will be discussed in the remainder of this section.

2.1. Minimizing the cost of the compressible simulation by CBSBC

By its nature, the compressible simulation captures the coupling between the fluctuating heat release rate and the acoustics. However, the plenum length L determines the thermoacoustic instability of the system. Hence, in order to capture the instability with the compressible simulation the full plenum length has to be modeled. Complex flow phenomena are restricted to the area contraction and the combustion zone. Inside the plenum only plane acoustic waves are propagating. Comparing the height of the area where the flame was observed during the thermoacoustic instabilities of about 40 mm with the total length of the plenum of up to 1 m, it becomes evident that resolving the full configuration with a CFD simulation would be a waste of computational resources. Therefore, in the present study we utilize the Characteristic Based State-Space Boundary Conditions (CBSBC) proposed in [7] to virtually extend the plenum to the full plenum length (compare Fig. 2).

CBSBC are a robust implementation of time domain impedance boundary conditions. They ensure that the CFD simulation follows the reflection coefficient imposed, accurately. CBSBC require a model of the reflection coefficient in state-space representation. Subsequently, we will first explain how the state-space model for the present study is determined. Afterwards, we show how the model is coupled with the compressible CFD simulation.

Plane acoustic waves can be described by means of the characteristic waves amplitudes

$$f = \frac{1}{2} \left(\frac{p'_A}{\rho c} + u'_A \right), \quad g = \frac{1}{2} \left(\frac{p'_A}{\rho c} - u'_A \right). \quad (2.1)$$

with density $\bar{\rho}$, speed of sound \bar{c} . p'_A and u'_A are the acoustic pressure and velocity fluctuations, respectively. f corresponds to the wave traveling in downstream direction and g to the wave traveling in upstream direction. The advection equations

$$\frac{\partial f}{\partial t} + (\bar{u} + \bar{c}) \frac{\partial f}{\partial x} = 0, \text{ and } \frac{\partial g}{\partial t} + (\bar{u} - \bar{c}) \frac{\partial g}{\partial x} = 0 \quad (2.2)$$

describe the propagation of the acoustic wave amplitudes. At inlet of the acoustic model the boundary condition

$$f(x = 0) = g(x = 0) \quad (2.3)$$

models a rigid wall. At the outlet of the acoustic model the boundary condition

$$g(t, x = L_A) = g_u(t) \quad (2.4)$$

allows to impose an arbitrary incoming wave $g_u(t)$. The discretization of (2.2) in space with the boundary conditions (2.3) and (2.4) can be written in state-space form

$$\dot{\mathbf{x}}_{comp} = A_{comp} \mathbf{x} + B_{comp} g_u \quad (2.5a)$$

$$f_u = C_{comp} \mathbf{x}_{comp} \quad (2.5b)$$

With the state-space matrices A_{comp} , B_{comp} , and, C_{comp} and the state-vector x_{comp} . The index ‘‘comp’’ emphasizes that the state space model belongs to the compressible simulation. For a detailed explanation of how these matrices can be determined we refer to [7].

The second step is to couple the model (2.5) with the CFD simulation. Here CBSBC extends the well-known Navier-Stokes characteristic boundary conditions (NSCBC) [10]. As in the NSCBC frame work CBSBC define the derivative of pressure p and velocity u according to

$$\frac{\partial p}{\partial t} + \frac{1}{2} (\mathcal{L}_5 + \mathcal{L}_1) = 0, \quad \frac{\partial u}{\partial t} + \frac{1}{2\rho\bar{c}} (\mathcal{L}_5 - \mathcal{L}_1) = 0. \quad (2.6)$$

Here, \mathcal{L}_5 and \mathcal{L}_1 are the temporal derivatives of the characteristic wave amplitudes f and g , respectively. \mathcal{L}_1 corresponds to the wave leaving the CFD domain and is given as

$$\mathcal{L}_1 = (u - c) \left(\frac{\partial p}{\partial x} - \rho c \frac{\partial u}{\partial x} \right). \quad (2.7)$$

\mathcal{L}_5 corresponds to the f -wave entering the domain and has to be imposed

$$\mathcal{L}_5 = \sigma \bar{\rho} \bar{c} (u - (f_u - g_d) - u_T) + \frac{\partial f_u}{\partial t}, \quad (2.8)$$

The term $(f_u - g_d)$ is equal to the acoustic velocity fluctuation. It avoids artificial reflections at the boundaries of the CFD domain by removing the acoustic velocity fluctuation from the relaxation term. The term $\partial f_u / \partial t$ allows to impose an ingoing wave. Please note, equation (2.8) is equal to the formulation given in [11].

Solving equations (2.5) to (2.8) in every time step allows to virtually extend the CFD domain to the full plenum length. Please note, by changing the length L_A we can change the plenum length without the requirement of a new mesh.

The fully compressible simulations were conducted using AVBP (Cerfacs and IFP).

2.2. Coupling of the incompressible simulation with an acoustic model

In contrast to the compressible simulation an incompressible simulation does not capture the thermoacoustic coupling. Even if the CFD domain were extended to the full

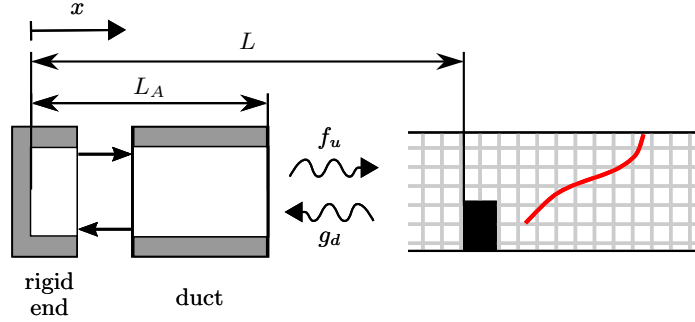


FIGURE 2. Coupling of the fully compressible simulation and the corresponding acoustic model.

plenum length, no thermoacoustic instability could be observed. Therefore, we couple the incompressible simulation with an acoustic network model using the Rankine-Hugoniot equations [12], as shown in Fig. 3.

The network model and the incompressible simulation are coupled via the global heat release rate \dot{q}' and a reference velocity u_{ref} . As the acoustic model is linear it can be written in state space form

$$\dot{\mathbf{x}}_{ico} = A_{ico}\mathbf{x}_{ico} + B_{ico}\dot{q}' \quad (2.9a)$$

$$u_{ref} = C_{ico}\mathbf{x}_{ico} + D_{ico}\dot{q}' \quad (2.9b)$$

With the state-space matrices A_{ico} , B_{ico} , and C_{ico} and the state-vector x_{ico} . Here, the index ‘‘ico’’ emphasizes that the state space model belongs to the incompressible simulation. A detailed description of how these matrices are determined can be found in [13]. The elements of the network model are shown in Fig. 3. As for the compressible case the duct sections were modeled using the linearized Euler equations. The model for the area jump is based on the continuity equation and does not include acoustic losses. The rigid end corresponds to a reflection coefficient of 1.

The Rankine-Hugoniot equations assume an infinitesimal thin flame. Although being compact with respect to the acoustic wave length, the flame in the incompressible simulation has a spatial extent. Therefore, a reference position at which the heat release is imposed to the acoustic field and a reference position at which the reference velocity is measured have to be selected. Both reference positions do not need to coincide. For the present study the reference for the heat release rate was chosen 2.6 mm after the second area jump. Two different reference positions for the velocity were investigated: (1) 15 mm upstream of the first area jump. This position coincides with the inlet of the incompressible simulation and is denoted as reference 0 (compare Fig. 3 and table 4). (2) The reference velocity was taken right in front of the area jump. In Fig. 3 and table 4 this position is denoted as reference 1.

The open-source code OpenFOAM was used as incompressible CFD solver.

3. Numerical results

The CFD settings for which self-excited thermoacoustic instabilities were simulated are shown in table 4. Simulations with a low and a high initial condition were conducted. The CFD field for the cases with a low perturbation of the initial field is the position of the steady flame. Only a small perturbation in the acoustic field has been imposed in order to speed up the development of a thermoacoustic instability. The simulations with

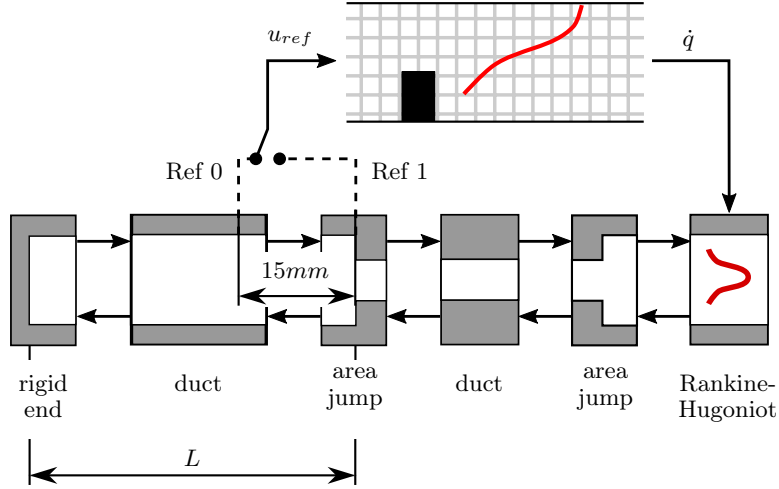


FIGURE 3. Coupling of the incompressible simulation and the corresponding acoustic model. The reference velocity is measured at two different locations (compare table 4).

case name	type	initial condition	reference position
CombLow	compressible	low perturbation	—
CombHigh	compressible	high perturbation	—
IcoLowRef0	incompressible	low perturbation	0
IcoHighRef0	incompressible	high perturbation	0
IcoHighRef1	incompressible	high perturbation	1

FIGURE 4. Compressible and incompressible CFD setups. Compare Fig. 3 for the reference position of the incompressible simulation.

high initial perturbation were started from a snapshot taken while the flame exhibited a thermoacoustic instability. The two different reference position for the incompressible simulation were explained in the previous section and are shown in Fig. 3.

In the remainder of this section we first compare the simulations by means of a bifurcation analysis. Thereafter, we have a close look at cases with a plenum length of $L = 200 \text{ cm}$ and $L = 700 \text{ cm}$.

3.1. Bifurcation analysis

The bifurcation diagram in terms of the root mean square (RMS) value of the velocity fluctuation is shown in Fig. 3.1. In general all simulations show good agreement. For long plenum length the error increases. The reason for this are the very high amplitudes of the oscillations observed. The corresponding velocities are so high that turbulent structures are generated. Therefore, the two dimensional assumption becomes questionable and, considering that two different CFD solvers are utilized, better agreement can not be expected.

It is interesting to note that the simulations with and without initial perturbation yield the same limit cycles. In contrast to experiments [1] and also models using the G-equation [5] hysteresis is not observed. For the discrepancy with experiment, several possible reasons can be named: E.g. the assumption of symmetry, the neglect of conjugate heat transfer, (unsteady) uncertainties in the boundary conditions and the

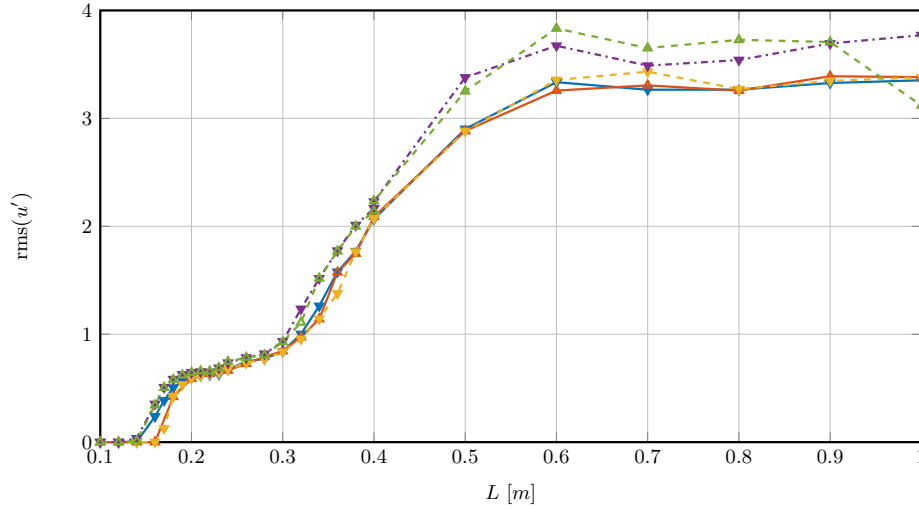


FIGURE 5. RMS values of the velocity fluctuation for different plenum length. —▲—: IcoLowRef0, —▼—: IcoHighRef0, —▲—: IcoHighRef1, —▼—: CombHigh, —▲—: CombLow

flow properties. Fewer reasons can be found to explain the difference to the G-equation simulation. Most likely are the different working conditions and the different geometry (both can also be reason for the mismatch with experiment). Here, a more intense parameter study is required which is planned in future investigations.

Another interesting point is the onset of the instability. It is observed that the compressible simulations and the incompressible simulation with reference position 1 (compare Fig. 3) become unstable at a plenum length of $L = 160mm$. The incompressible simulations with reference position 0, however, exhibit an instability starting at a plenum length of $170mm$. Therefore, the less intuitive coupling using a reference position which is right before the area jump is more accurate than the coupling using a reference position that coincides with the inlet of incompressible simulation. The reason is that due to incompressibility, a velocity fluctuation imposed at the inlet will act on the whole CFD domain, immediately. Therefore, the reference position should be chosen at the place where acoustic fluctuations create hydrodynamic fluctuations, which most often does not coincide with the position of the inlet of the CFD domain.

In Fig. 3.1 the dominant frequency f_u of the unstable working points are shown. In general a very good agreement is observed. Only for short plenum length the incompressible simulation slightly unpredictably the dominant frequency.

3.1.1. Comparison of time series

In Fig. 7, 8 the time series and the power spectrum for a plenum length of $200mm$ and $700mm$ are shown. Both plots show that the simulations are in good agreement with each other. In agreement with the bifurcation diagram, the amplitude at a plenum length of $700mm$ is significantly larger than the amplitude at $L = 200mm$. In the power spectrum for $L = 700mm$ a noise content is observed, which can be attributed to the onset of turbulence due to the high oscillation amplitudes.

The configuration considered is nonlinear and the behavior of a nonlinear system is better understood with the help of phase portraits. Phase portraits represent the asymptotic state of the system in the phase space. We can construct the phase space once we

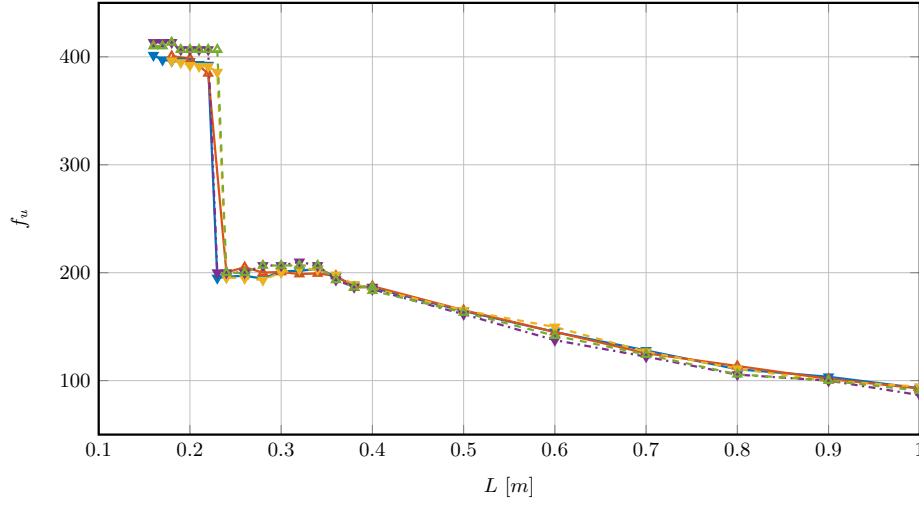


FIGURE 6. Dominant frequency of the velocity signal for different plenum length. —▲—: IcoLowRef0, —▼—: IcoHighRef0, —▲—: IcoHighRef1, —▼—: CombHigh, —▲—: CombLow

have the knowledge of the variables which govern the dynamics of the system. Often a complete information of the governing equations will not be available and we will have access to just one state space variable. Even in cases where we have access to only one state space variable, we can reconstruct the phase space by applying Takens' embedding theorem [14]. In order to reconstruct the phase space, we will create n delayed vectors from the available time series, where each vector will be delayed by τ . The most important parameters to be determined are the optimum delay and the minimum embedding dimension. The optimum delay will correspond to the first minima of the average mutual information and the minimum embedding dimension can be found using the method of false nearest neighbors. A detailed description of the techniques involved in the phase space reconstruction in the context of a thermoacoustic system can be found in [15]. As shown in Fig. 9, also the phase portraits of the simulations are in good agreement. From the phase portrait we can also deduce the nature of the oscillation observed: We are observing Period-2 oscillations at $L = 20 \text{ cm}$ and limit cycle oscillations at $L = 70 \text{ cm}$.

4. Conclusion

In the present study two different CFD-based, nonlinear, time-domain models of self-excited thermoacoustic instabilities of a laminar premixed flame (see Fig. 1) are compared: The first model (see Fig. 2) resolves the flame with a fully compressible simulation. In order to minimize the CFD domain and thus the computational costs required, the plenum is modeled using a one dimensional acoustic description. CBSBC [7] are used to couple the compressible simulation with the low order model. The second model (see Fig. 3) uses an incompressible code to describe the flame dynamics. This simulation is coupled with an acoustic network model according to the Rankine-Hugoniot equations.

A bifurcation analysis using the plenum length as bifurcation parameter is conducted. Both models are in good agreement with each other. In contrast to numerical studies based on the G-equation hysteresis is not observed. As the flame models used in the present study are significantly more complex than the G-equation, the most likely reason

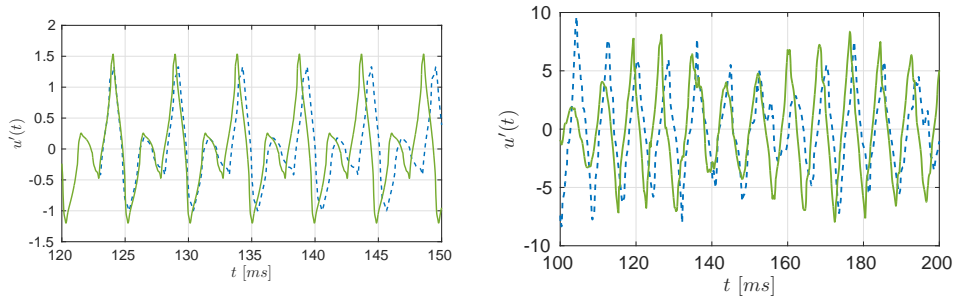


FIGURE 7. Time series of the velocity signal for $L = 200$ mm (left) and $L = 700$ mm (right). —: Compressible simulation, - - -: Incompressible simulation

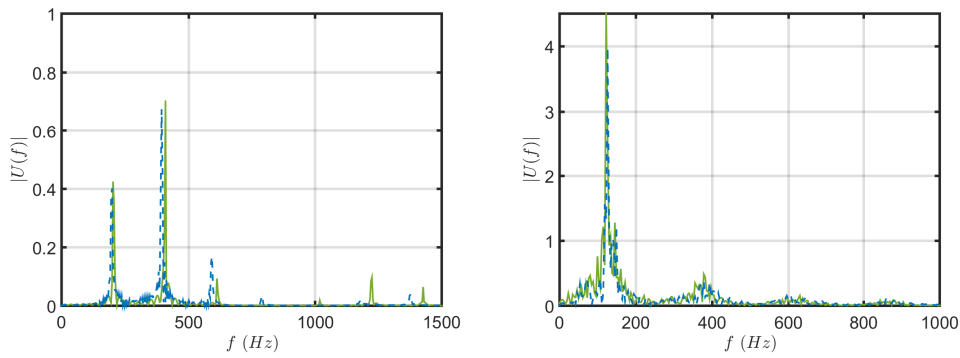


FIGURE 8. Power spectrum of the velocity signal for $L = 200$ mm (left) and $L = 700$ mm (right). —: Compressible simulation, - - -: Incompressible simulation

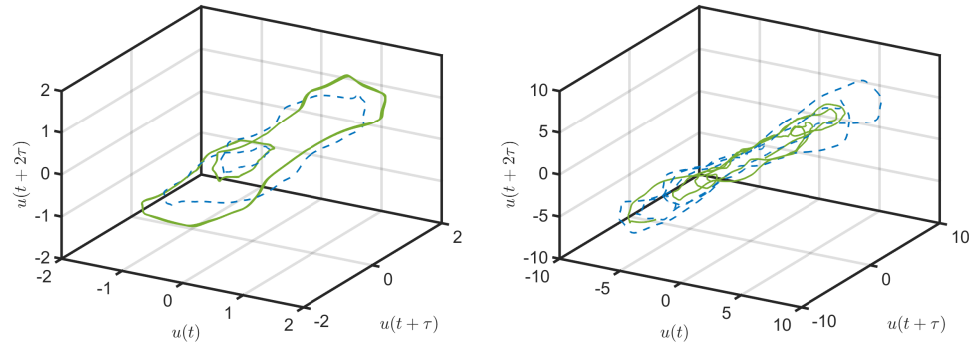


FIGURE 9. Phase portrait of the velocity signal for $L = 20$ cm (left) and $L = 70$ cm (right). —: Compressible simulation, - - -: Incompressible simulation

for this are different working conditions and a different geometry of the flame holder. Therefore, a more comprehensive bifurcation analysis is required. As it was shown in the present work that both simulations are in good agreement this study can be conducted only with one of the simulations. This reduces the computational costs and thus, allows a more extensive parameter study.

The models investigated in the present study form a basis for further research. On the one hand they can be compared with experimental results and if necessary be extended.

On the other hand they can serve as reference for nonlinear reduced-order models for the dynamics of laminar flames.

5. Acknowledgment

The financial support for the first author has been provided by the Research Association for Combustion Engines (Forschungsvereinigung Verbrennung e.V - FVV, project number: 6011150). Financial support for the second author has been provided by the German Research Foundation (DFG) and for the third author by the DFG in the framework of the DFG TRR40. This support is gratefully acknowledged. We thank CERFACS and IFP for providing the solver AVBP. The authors gratefully acknowledge the Gauss Centre for Supercomputing e.V. (www.gauss-centre.eu) for funding this project by providing computing time on the GCS Supercomputer SuperMUC at Leibniz Supercomputing Centre (LRZ, www.lrz.de).

References

- [1] KABIRAJ, L., SUJITH, R.I., AND WAHI, P. (2012). *Bifurcations of self-excited ducted laminar premixed flames*. *J. Eng. Gas Turb. Power*, **134**, 031502.
- [2] DOWLING, A. P. (1999). *A Kinematic Model of a Ducted Flame*. *J. Fluid Mech.*, **394**, 51–72.
- [3] NOIRAY, N., DUROX, D., SCHULLER, T. AND CANDEL, S. (2008). *A unified framework for nonlinear combustion instability analysis based on the flame describing function*. *J. Fluid Mech.*, **615**, 139–167.
- [4] KASHINATH, K., HEMCHANDRA, S., AND JUNIPER, M.,P. (2013). *Nonlinear phenomena in thermoacoustic systems with premixed flames*. *J. Eng. Gas Turb. Power*, **135**, 061502.
- [5] KASHINATH, K., WAUGH, I.,C. AND JUNIPER, M.,P. (2014). *Nonlinear self-excited thermoacoustic oscillations of a ducted premixed flame: bifurcations and routes to chaos*. *J. Fluid Mech.*, **761**, 399–430.
- [6] ORCHINI, A., ILLINGWORTH, S.,J. AND JUNIPER, M.,P. (2015). *Frequency domain and time domain analysis of thermoacoustic oscillations with wave-based acoustics*. *C. U. P.*, **775**.
- [7] JAENSCH, S., SOVARDI, C., AND POLIFKE, W. (2015). *Imposing frequency dependent reflection coefficients at the boundary of a compressible flow simulation by coupling state-space models via characteristics*. *submitted to J. Comp. Phys.*, .
- [8] KORNILOV, V. N., ROOK, R., TEN THIJE BOONKKAMP, J. H. M., DE GOEY, L. P. H. (2009). *Experimental and numerical investigation of the acoustic response of multi-slit Bunsen burners*. *Combust. Flame*, **156**, 1957–1970.
- [9] DUCHAINE, F., BOUDY, F., DUROX, D. AND POINSOT, T. (2011). *Sensitivity analysis of transfer functions of laminar flames*. *Combust. Flame*, **158**, 2384–2394.
- [10] POINSOT, T. AND LELE S.,K. (1992). *Boundary conditions for direct simulation of compressible viscous flows*. *J. of Comput. Phys.*, **101**, 104–129.
- [11] POLIFKE, W. WALL, C. AND MOIN, P. (2006). *Partially reflecting and non-reflecting boundary conditions for simulation of compressible viscous flow*. *J. of Comput. Phys.*, **213**, 437–449.
- [12] CHU., B. T. (1953). *On the generation of pressure waves at a plane flame front*. In: *Proceedings of the 4th Symposium (International) on Combustion*, **4**, 603–612.

- [13] EMMERT, T., JAENSCH, S., SOVARDI, C., AND POLIFKE, W. (2014). *taX - a flexible tool for low-order duct acoustic simulation in time and frequency domain*. 7th Forum Acusticum, Krakow, Poland.
- [14] TAKENS, F. (1981). *Detecting strange attractors in turbulence*. Springer .
- [15] KABIRAJ, L. AND SUJITH, R. I. (2012). *Nonlinear self-excited thermoacoustic oscillations: intermittency and flame blowout*. *J. Fluid Mech.*, **713**, 376–397 .